TU Delft

Delft University of Technology

Rheology of flexible fiber-reinforced cement pastes

Maximum packing fraction determination and structural build-up analysis

Guo, Zhenbang; Qiu, Jingping; Huang, Duanping; Liu, Kai; Kirichek, Alex; Liu, Chen; Chen, Boyu; Zhao, Yingliang; Qu, Zhengyao

DOI
10.1016/j.compstruct.2024.118662

Publication date
2024

Document Version
Final published version

Published in
Composite Structures

Citation (APA)
Guo, Z., Qiu, J., Huang, D., Liu, K., Kirichek, A., Liu, C., Chen, B., Zhao, Y., & Qu, Z. (2024). Rheology of flexible fiber-reinforced cement pastes: Maximum packing fraction determination and structural build-up analysis. *Composite Structures*, *352*, Article 118662. https://doi.org/10.1016/j.compstruct.2024.118662

Important note
To cite this publication, please use the final published version (if applicable).
Please check the document version above.

Copyright
Other than for strictly personal use, it is not permitted to download, forward or distribute the text or part of it, without the consent of the author(s) and/or copyright holder(s), unless the work is under an open content license such as Creative Commons.

Takedown policy
Please contact us and provide details if you believe this document breaches copyrights.
We will remove access to the work immediately and investigate your claim.

This work is downloaded from Delft University of Technology.
For technical reasons the number of authors shown on this cover page is limited to a maximum of 10.

Green Open Access added to TU Delft Institutional Repository

'You share, we take care!' - Taverne project

https://www.openaccess.nl/en/you-share-we-take-care

Otherwise as indicated in the copyright section: the publisher is the copyright holder of this work and the author uses the Dutch legislation to make this work public.

Composite Structures 352 (2025) 118662

Contents lists available at ScienceDirect

Composite Structures

journal homepage: www.elsevier.com/locate/compstruct

Response to comments on

Rheology of flexible fiber-reinforced cement pastes: Maximum packing fraction determination and structural build-up analysis

Zhenbang Guo [a,b,c], Jingping Qiu [b], Duanping Huang [d,e], Kai Liu [d], Alex Kirichek [c], Chen Liu [f], Boyu Chen [f], Yingliang Zhao [g], Zhengyao Qu [a,*]

[a] State Key Laboratory of Silicate Materials for Architectures, Wuhan University of Technology, Wuhan 430070, China
[b] School of Resource and Civil Engineering, Northeastern University, Shenyang 110819, China
[c] Section of Rivers, Ports, Waterways and Dredging Engineering, Department of Hydraulic Engineering, Faculty of Civil Engineering & Geosciences, Delft University of Technology, Stevinweg 1, 2628 CN Delft, Netherlands
[d] School of Materials Science and Engineering, Wuhan University of Technology, Wuhan, 430070, China
[e] Advanced Ceramics Institute of Zibo New & High–Tech Industrial Development Zone, Zibo, 255000, China
[f] Department of Materials and Environment (Microlab), Faculty of Civil Engineering and Geoscience, Delft University of Technology, Delft, the Netherlands
[g] Department of Civil and Environmental Engineering, The Hong Kong Polytechnic University, Hung Hom, Kowloon, Hong Kong, China

ARTICLE INFO

Keywords
Flexible fiber
Cement paste
Maximum packing fraction
Static yield stress
Structural build-up

ABSTRACT

The maximum packing fraction (φ_{fm}) of flexible fibers is an essential parameter for understanding the rheological behavior of flexible fiber-reinforced cement paste (FFRCP). However, direct measurement of φ_{fm} of flexible fibers is still lacking. In this study, a shear rheology-based method for direct measurement of φ_{fm} was proposed and the assumption of fiber conformation under shear was verified by micro-CT. Based on this, a yield stress model for FFRCP was constructed to explain the entanglement and friction effects in the fiber network. Finally, static yield stress tests and small amplitude oscillatory shear (SAOS) tests were carried out to explore the structural build-up of FFRCP. It was found that the proposed method enables direct determination of φ_{fm} through only a few viscosity-fiber content data for a given FFRCP. Furthermore, the proposed model can describe the static yield stress of FFRCP well. Finally, the relative structural build-up rate of FFRCP follows a similar trend as the relative yield stress, with a critical relative fiber volume fraction (0.299) as the boundary. Subsequently, the relative structural build-up gradually deviates from the relative yield stress due to the limiting effect of the fibers.

1. Introduction

Synthetic flexible fibers such as polypropylene (PP) fibers have proven to be a versatile addition to cement paste [1–4]. The incorporation of flexible fibers contributes to enhancing the crack resistance, toughness, and dimensional stability, leading to an improvement in the overall durability and service life of the cement-based materials [5–9]. However, like rigid fibers, the inclusion of flexible fibers is detrimental to the workability of fresh cement-based materials, particularly at high fiber content [10–12]. Workability, which is dependent on rheological properties, is a fundamental property of cement-based materials and its control ensures correct and easy casting [13–15]. Specifically, the workability also plays a crucial role in the interlayer interface properties of 3D printed fiber-reinforced cement-based materials (FRCBM) [16–18].

The effects of fiber type, fiber content, fiber geometry and fiber orientation on the workability or rheological properties of cement-based materials have been investigated in numerous studies [12,14,19–24]. It was generally found that the primary determinant of the fresh properties of FRCBM is the maximum packing fraction of the fibers. However, predicting the rheological properties of cement-based materials containing synthetic flexible fibers remains a challenging task. Sultangaliyeva et al. [20] proposed a yield stress model for cementitious materials based on fiber content and geometry, elastic modulus, and the rheology of suspension. This model provides a profound understanding of the deformation and orientation of flexible fibers in cement-based materials. However, on the one hand the key to predicting fiber-induced amplification of the yield stress of the model lies in the maximum packing fraction of fibers as described, which in turn requires knowledge of the yield stress of suspension medium. On the other hand,

* Corresponding author.
E-mail address: quzhengyao@whut.edu.cn (Z. Qu).

https://doi.org/10.1016/j.compstruct.2024.118662
Received 27 November 2023; Received in revised form 10 March 2024; Accepted 19 October 2024
Available online 22 October 2024
0263-8223/© 2024 Elsevier Ltd. All rights are reserved, including those for text and data mining, AI training, and similar technologies.

the evaluation of maximum packing fraction in this model is not applicable to fiber samples with multiple sizes or different elastic moduli, such as hybrid fibers. Although the maximum packing fraction of fibers can be measured by dry packing method, it is sensitive to the applied compaction degree and cannot account for the effect of water in the cement-based materials [25]. The maximum packing fraction of flexible fibers is more accurately described as a contact percolation fraction rather than the "geometric" maximum packing density determined through compaction experiments [20]. It is noteworthy that Li et al. [19,21] investigated the packing density of mortar containing flexible fibers using the wet packing method [26,27]. But in fact, what is obtained is the packing density of the solid system when the flexible fibers were in a specific conformation. The flowing or mixing can induce a preferred orientation of the flexible fibers and thus modify the fresh properties of the cement-based materials [12]. This means that the conformation of the flexible fiber changes dynamically during the shearing process, in other words the packing fraction of the flexible fibers is not fixed either. The dynamic properties of flexible fibers in cement-based materials under shearing has been rarely reported previously. In summary, it is necessary to propose a method that can directly measure the maximum packing fraction of flexible fibers while also reflecting the dynamic characteristics of the packing fraction under shear.

After the maximum packing fraction of the fibers is determined, the modeling of the rheological properties of FRCBM can be performed. Some yield stress models for FRCBM based on multi-scale approaches have been proposed, which relate the yield stress of the suspending fluid and the fiber volume fraction to the yield stress of FRCBM [20,28,29]. However, it is important to remember that the underlying logic of these models, i.e., the yield stress of FRCBM is proportional to the constitutive cement paste, is historically established for semi-dilute systems [12]. That is to say, only the hydrodynamic interactions between the suspending fluid and the inclusions are considered, so it is theoretically unsuitable for high-concentration cement-based suspensions. This means that the modeling of yield stress in FRCBM needs to be further improved to provide deeper insights, especially when the higher content of flexible fibers results in entanglement and friction effects in the fiber network that are not negligible.

As mentioned earlier, the literature on the yield stress of FRCBM is abundant, but studies focusing on the time-dependent rheological behavior or the structural build-up are limited. The thixotropic structural build-up of cement-based materials is an intrinsic property that plays an important role in pumpability, stability and formwork filling as well as buildability for 3D printing [30]. Although Perrot et al. [31] developed a structural build-up model for FRCBM, it was targeted specifically towards rigid fibers. Chen et al. [32] studied the static yield stress evolution of 3D printed calcium sulphoaluminate cement composites (CSACCs) with polypropylene (PP) and polyvinyl alcohol (PVA) fibers. This has certain guiding significance for the study of FRCBM structural build-up, but the relationship between structural build-up and fiber properties, especially the maximum packing fraction, is lacking. This is not conducive to further understanding of the structural build-up of FRCBM. Therefore, the structural build-up for cement-based materials containing flexible fibers requires further research.

This study aims to develop a new experimental method that can be used to measure the maximum packing fraction of flexible fibers directly. Based on this, it is hoped that a yield stress model can be constructed that will provide deeper insights into the contribution of fibers in flexible fiber-reinforced cement paste (FFRCP). Finally, the structural build-up of the FFRCP was explored.

2. Methodology

Inspired by the structural response of flocs under shear [33,34], flexible fibers can be considered as a special type of floc that undergoes shape and orientation changes under shear, resulting in alterations to the rheological properties of FFRCP. The specific methodology for this proposed approach is outlined below:

Sultangaliyeva et al. [20] developed a model based on [12], Eq. (1) below, which was confirmed to be capable of predicting the yield stress of FFRCP. This model implies that an increase in yield stress of FFRCP (τ_0) is due to the increase of fiber volume fraction (φ_f), and furthermore, as φ_f tends to the maximum packing fraction (φ_{fm}), $\tau_0 \to \infty$.

$$\frac{\tau_0}{\tau_{00}} = \left(1 - \frac{\varphi_f}{\varphi_{fm}}\right)^{-2} \tag{1}$$

where τ_{00} is the yield stress of the suspension medium, i.e., the pure cement paste.

According to rheology, that is, viscosity is the ratio of shear stress to shear rate, Eq. (1) can also be written in the form of viscosity as:

$$\frac{\eta_0}{\eta_{00}} = \left(1 - \frac{\varphi_f}{\varphi_{fm}}\right)^{-2} \tag{2}$$

where η_0 and η_{00} are the viscosities corresponding to τ_0 and τ_{00} respectively.

It should be noted that compared to rigid fibers, flexible or soft fibers do strongly deform when dispersed in cement-based materials [20]. The fibers gradually deviate from the conformation and orientation corresponding to dense packing with deformation, thus reducing the maximum packing fraction. As a result, the viscosity of FFRCP will increase due to the decrease of water film thickness [19]. Here, Eq. (2) can be extended to account for the effect of such fiber deformation on the rheological properties of FFRCP.

As the deformed fibers are subjected to increasing shear stress (τ), the fibers will straighten and rearrange. In this case, preferential fiber orientation along a given shear direction is expected to occur within a FFRCP element [35]. And φ_{fm} is more representative of the packing fraction for fibers at a certain deformation state. The preferred fiber conformation and orientation corresponding to φ_{fm} will be achieved only when the applied shear rate or stress is large enough (usually assumed to be infinite) [12]. Therefore, Eq. (2) should be reformulated taking into account the shear-induced change in fiber deformation. Furthermore, φ_{fm} becomes the effective maximum packing fraction ($\varphi_{fmeff}(\tau)$), which is a function depending on shear stress or rate. This effective maximum packing fraction accounts for the increase of fiber deformation. A schematic evolution of $\varphi_{fmeff}(\tau)$ versus shear stress is presented in Fig. 1. It should be emphasized that φ_f is a fiber volume fraction, not an effective volume fraction, since fibers at low

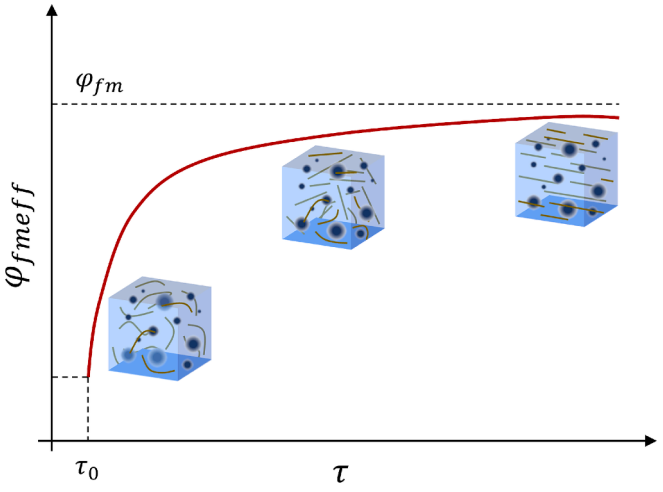

Fig. 1. Evolution of the effective maximum packing fraction $\varphi_{fmeff}(\tau)$ for flexible fibers as a function of shear stress τ.

concentrations (to which this method is applicable) do not trap free water like particle flocs, resulting in an increase in the actual volume fraction [36]. As for the reason why the proposed method is based on the premise of low fiber content, it will be explained later. In addition, Eq. (2) is essentially a special case of the Krieger and Dougherty model [37], that is, the exponent is −2. But this also results in a loss of flexibility in fitting experimental data [34]. Therefore, an adjusting parameter "a" (following Tregger et al. [33]) is introduced to increase the flexibility of the model. As a result, Eq. (2) can be expressed in more appropriate form as the following Eqs. (3) and (4) for FFRCP.

$$\eta'(\tau) = \left[a\left(1 - \frac{\varphi_f}{\varphi_{fmeff}(\tau)}\right)\right]^{-2} for \tau > \tau_0 \quad (3)$$

and,

$$\eta' = \left[a'\left(1 - \frac{\varphi_f}{\varphi_{fm}}\right)\right]^{-2} for \tau \to \infty (\tau \gg \tau_0) \quad (4)$$

where $\eta'(\tau)$ is the ratio of the viscosity of the FFRCP to that of the suspension medium, and the value depends on τ. η' and a' are the corresponding viscosity ratio and adjusting parameter when $\tau \gg \tau_0$, respectively.

Based on Eqs. (3) and (4), together with the method developed by Liu [34], $\varphi_{fmeff}(\tau)$ and φ_{fm} can be determined. Firstly, the stress ramp-up tests are performed to obtain the flow curves of cement pastes with different initial fiber volume fractions (Fig. 2**(a)**). Subsequently, the $1-[\eta'(\tau)]^{-1/2}$ value corresponding to a given shear stress (τ_1) is plotted against the fiber volume fraction, which can be fitted linearly, as shown in Fig. 2**(b)**. When $\eta'(\tau)$ tends to infinity, φ_f is close to $\varphi_{fmeff}(\tau)$, and the $1-[\eta'(\tau)]^{-1/2}$ value tends to 1. Hence, the $\varphi_{fmeff}(\tau_1)$ for the given stress value is achieved when $1-[\eta'(\tau_1)]^{-1/2} = 1$. Repeating this for each stress value yields the $\varphi_{fmeff}(\tau) - \tau$ curve, and φ_{fm} corresponds to the $\varphi_{fmeff}(\tau)$ value when $\tau \gg \tau_{00}$ (Fig. 2**(c)**). Fig. 3 shows a flowchart of the shear rheology-based method for φ_{fm} measurement.

3. Experimental materials and methods

The materials used in this study for the preparation of FFRCP included cement, flexible fibers and water. The cement used was commercial ordinary Portland cement (PO 42.5R) conforming to GB175-2007, with specific gravity and specific surface area of 3.3 and 355 m^2/kg respectively. The main chemical composition of PO 42.5R is CaO (64.9 %), SiO_2 (22.3 %), Al_2O_3 (4.2 %) and Fe_2O_3 (3.6 %), etc. More detailed information on the physical and chemical properties of cement can be found in [38]. The flexible fibers studied were polypropylene (PP) fibers. According to the classification criterion defined by Martinie et al. [12], the fibers can be considered as flexible fibers. Table 1 shows some basic parameters of the PP fibers. In addition, tap water from the laboratory was used as mixing water.

3.1. Mix proportions and sample preparation

The water-to-cement ratio (W/C) for the samples subjected to maximum packing fraction tests and rheological tests was 0.5. Due to the relatively prolonged duration required by the micro-CT test, in order to minimize the influence of bleeding and settlement while maintaining a reasonably close W/C used in other tests, a W/C of 0.5 has been chosen for the micro-CT test. For the maximum packing fraction test, two different volume fractions for each fiber were required to determine the maximum packing density. Concerning the static yield stress test, the fiber volume content was set at 1, 2 and 3 %, regardless of the aspect ratio. In addition, the fiber content was fixed at 1 % for the small amplitude oscillatory shear (SAOS) test. The detailed mix designs of the FFRCP are summarized in Table 2.

Once the pre-set ingredients have been weighed, the water was first added to the cement and mixed in the mixer (NJ-160A) bowl for 2 min. Subsequently, PP fibers were divided into three portions and slowly fed into the cement paste by hand to ensure proper distribution and minimize fiber clumping effects [29]. The cement paste was mixed for another 1 min to obtain the final FFRCP mixture.

3.2. X-ray micro-CT test

X-ray micro-CT technique (ZEISS Xradia 510 Versa 3D X-ray microscope, 120 kV and 10 W) was selected in this study to capture the orientation and distribution of fibers in cement paste. The cement paste samples with W/C of 0.5 were tested immediately after shearing. In addition, a low fiber volume fraction of 0.1 % was maintained to ensure the better independent distinction of each fiber [20]. Three samples, denoted as CT-0, CT-10, and CT-20, were prepared and subjected to shear at a rate of 10 Pa/s for 0 s, 10 s, and 20 s, respectively, followed by CT scanning tests. After 2D image processing, the XCT VG Studio MAX software was used for the reconstruction of 3D images. The method in [39] was employed to extract the information on the coordinates and angles of fibers in 3D space. Finally, the average ratio of the fiber length in the shearing direction to the original fiber length was defined as the orientation factor to quantify the fiber orientation [39].

3.3. Maximum packing fraction test

The stress ramp-up protocol was performed using a Brookfield rheometer (RSX-SST) to determine the flow curves for maximum packing fraction test of flexible fibers. The rheometer's torque and speed ranges are 0.1–200 mNm and 0.01–1000 rpm, respectively. The rotator used was a four-bladed vane with a length and diameter of 40 mm and 20 mm respectively. The FFRCP samples were tested directly after being moved to the cup (1000 mL beaker). To avoid strongly modifying the

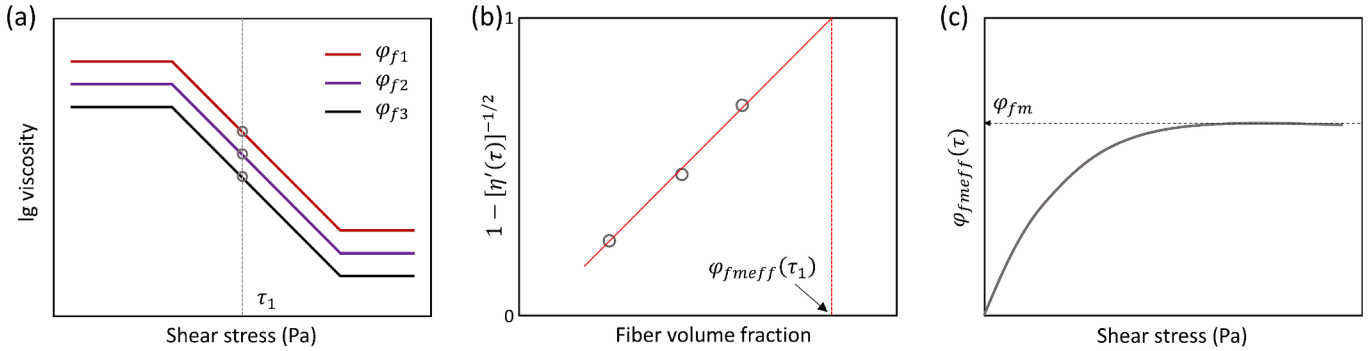

Fig. 2. (a) Flow curves of cement pastes containing different fiber contents (φ_{f1}, φ_{f2}, φ_{f3}); (b) Determination of $\varphi_{fmeff}(\tau_1)$; (c) Determination of the maximum packing fraction φ_{fm}.

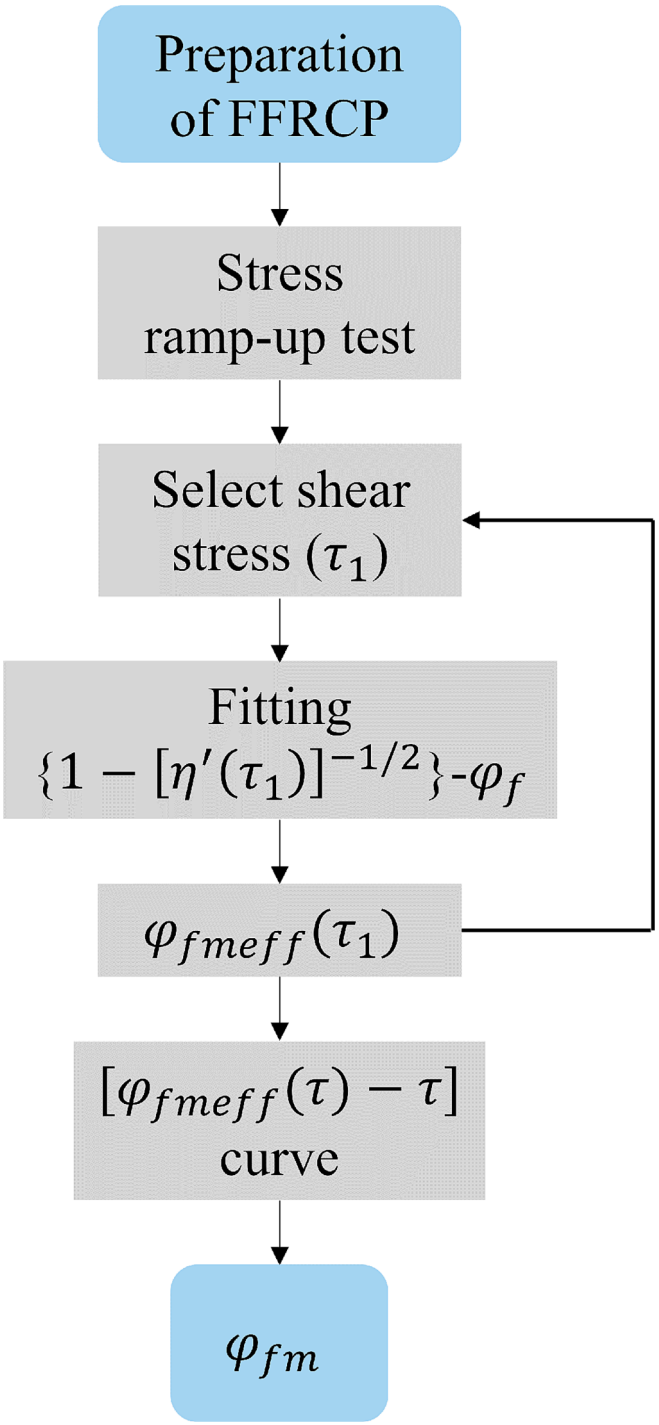

Fig. 3. A flowchart of the proposed shear rheology-based method.

orientation of fibers, no pre-shear step was performed before tests [12]. The shear stress was increased linearly from 0 to 250 Pa at a rate of 10 Pa/s. The resultant shear stress versus viscosity curves were recorded. The $1-[\eta'(\tau)]^{-1/2}$ versus φ_f curves were plotted and extrapolated to a value of 1 for each shear stress to obtain φ_{fmeff}. Finally, φ_{fm} was obtained according to the evolution result of φ_{fmeff} with shear stress. The temperature of the sample was controlled at ~20 °C by a water bath device.

3.4. Static yield stress test

The rheometer and rotor used for static yield stress test are consistent with the maximum packing fraction test described above. To obtain the static yield stress of FFRCP just after mixing, a constant shear rate (0.1 s^{-1}) protocol was adopted. The applied shear rate is consistent with previous studies as reported in [40]. The peak of the shear stress evolution was taken as the static yield stress. Each yield stress test was performed three times to ensure the repeatability of the measurements. Note that transferring the prepared fresh FFRCP to the rheometer requires a slow pouring velocity to avoid effect on the fiber orientation [31]. Similarly, no pre-shear step was carried out before this test and the temperature was controlled at ~20 °C.

Further, the static yield stresses of the samples at resting times of 300, 720, 1200 and 1800 s were measured to evaluate the structural evolution of the FFRCP. Then the Roussel model [41] was used to obtain the structural build-up rate of the FFRCP (A_{thix}^{FFRCP}).

$$\tau_s = \tau_0 + A_{thix}^{FFRCP} \bullet t_{rest} \tag{5}$$

where τ_s is the static yield stress of the sample, t_{rest} is the resting time.

3.5. SAOS test

To obtain the evolution of the storage modulus (G′) and phase angle (δ), SAOS time sweep measurements were carried out in a rotational rheometer (Anton Paar MCR 302) with a concentric cylindrical geometry. The frequency was chosen as 1 Hz, which allowed sufficient time for the hydration products to build up and provided stable data [42]. In addition, strain amplitude sweeps were performed to determine the linear viscoelastic domain (LVED), where the storage modulus is independent of the applied shear strain. Finally, the angular frequency and strain amplitude were determined to be 1 Hz and 0.001 %, respectively, within LVED, for the subsequent time sweep test.

4. Results and Discussions

4.1. Initial validation of the shear rheology method

The primary premise for the validity of the proposed shear rheology

Table 2
Summary of the mix proportions of the FFRCPs prepared.

Experiment type	W/C	Fiber length (mm)	Fiber content (%)
X-ray micro-CT test	0.5	6	0.1
Maximum packing fraction test	0.6	3	0, 0.164, 0.185
		6	0, 0.068, 0.087
		9	0, 0.029, 0.046
		12	0, 0.043, 0.059
Static yield stress test	0.6	3	0, 1, 2, 3
		6	0, 1, 2, 3
		9	0, 1, 2, 3
		12	0, 1, 2, 3
SAOS test	0.6	3	0, 1
		6	0, 1
		9	0, 1
		12	0, 1

Table 1
Basic parameters of PP fibers.

Fiber type	Length (mm), L	Diameter (μm), D	Density (g/m^3)	Tensile strength (MPa)	Young's modulus (GPa), E	Elongation rate (%)
PP	3, 6, 9, 12	40	0.91	398	4.2	28.0

test method is the assumption that the fiber conformation undergoes continuous straightening and rearranging under shear. The purpose of this section is therefore to validate this hypothesis. The 3D CT-reconstructed images of the fibers under different shear conditions are shown in Fig. 4. As expected, these fibers do undergo deformation in the cement paste. However, due to the high W/C, the overall degree of fiber bending is not significant. This is consistent with the conclusion from [20]. When un-sheared, the fibers in the paste exhibited extremely non-uniform distribution (Fig. 4**(a)**). However, under the action of shearing, the fibers become increasingly dispersed and straightened (Fig. 4**(b) and (c)**). In the shear direction, with the increase of shear time, the orientation factor of fibers (the average ratio of the fiber length in a certain direction to the actual length of all flexible fibers [39]) increases gradually (0.54, 0.60 and 0.72), suggesting that fiber tends to lie more parallel to this direction. Therefore, the hypothesis was quantitatively validated by micro-CT imaging and 3D image reconstruction, which preliminarily demonstrated the rationality of the proposed shear rheology test method.

4.2. Maximum packing fraction

According to the assumptions of the background theory (Fig. 1), a relationship that increases first and then reaches a plateau exists between $\varphi_{fmeff}(\tau)$ and τ for the fresh FFRCP. This is confirmed for the FFRCP, as illustrated in Fig. 5**(a)**. It is worth noting that when the shear stress is less than 150 Pa, which is much larger than the yield stress of the suspension medium, that is, pure cement paste, the $\varphi_{fmeff}(\tau)$ of the fibers is hardly dependent on the shear stress regardless of the fiber length or aspect ratio. This plateau region did not occur when a similar shear rheology test method was used to measure the solid volume fraction of cement paste containing clay admixtures [33]. This distinction can be attributed to the fact that the flexible fibers can adapt to the shear by deformation, which means that more energy is required to achieve the yielding of system [43,44]. The fiber is gradually straightened and rearranged continuously under shearing, causing $\varphi_{fmeff}(\tau)$ to increase continuously until the optimal conformation is obtained, which corresponds to φ_{fm} of the fiber. Similar $\varphi_{fmeff}(\tau)-\tau$ relationship was also reported in highly concentrated calcium carbonate suspensions [45]. To quantify the dynamic characteristics of the flexible fiber under shearing and obtain φ_{fm} more accurately, a stretched exponential function was adopted:

$$\varphi_{fmeff}(\tau)=\varphi_{fmi}+(\varphi_{fm}-\varphi_{fmi})\left\{1-exp\left[-\left(\frac{\tau}{\tau_r}\right)^{k}\right]\right\} \tag{6}$$

where φ_{fmi} is the initial packing fraction of fibers before shearing. τ_r is the characteristic shear stress which reflects the resistance of the fibers to deformation. k is a coefficient reflecting the rate of change in fiber conformation with shear stress.

It should be noted that due to the influence of the mixing and transfer process on the fiber conformation, φ_{fmi}, τ_r and k may be inconsistent even for the same fiber, but φ_{fm} is unchanged. This is similar to the characteristic of cement-based materials reaching an equilibrium state under shearing as shown in [40]. Also, strictly speaking, the above conclusion regarding shear history-independent φ_{fm} applies only to

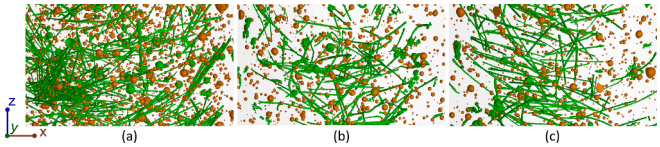

Fig. 4. 3D CT-reconstructed images of different samples: (a) CT-0; (b) CT-10; (c) CT-20. Green represents fibers and brown color represents pores. In addition, 0, 10 and 20 represent shearing times of 0 s, 10 s and 20 s respectively.

FFRCP under the critical shear intensity. Han and Ferron [46] discovered that upon reaching the threshold shear intensity, the cement paste displayed a shear-thickening behavior. Since the conformation of flexible fibers depends on the consistency of the cement paste [20], Eq. (6) holds only below a certain shear intensity. This also means that the fibers cannot always maintain the optimal conformation as the shear stress continues to increase.

As shown in Fig. 5**(a)**, the evolution of φ_{fmeff} with shear stress can be well described by the Eq. (6). The φ_{fm} of 3, 6, 9 and 12 mm PP fibers can be obtained as 0.0693, 0.0631, 0.0557 and 0.0484, respectively. Clearly, these packing fractions are all greater than the ones obtained with Sultangaliyeva model (see Eq. (9) in [20]), which were derived from the spread test results (see Fig. 5**(b)**). One explanation can be that the deformed fibers are not fully straightened and rearranged due to the low shear rates involved during the spread tests and thus the optimal fiber conformation is not obtained [47]. This maximum packing fraction gap also reflects the rationality of the proposed method. In addition, as expected, φ_{fm} decreases as the fibre aspect ratio (A) increases. Martinie et al. [12] showed that the dense packing fraction of rigid straight fibers with high aspect ratio scales with $1/A$. As flexible fibers deform in the cement paste and eventually quite different from original straight shape, the actual aspect ratio (A') can be expressed as the ratio of the effective length (L_{eff}, defined as the average distance between the ends of the deformed fiber) [20] to diameter of the fiber, which reads:

$$A^{'}\propto D^{-\frac{2}{5}}L^{\frac{1}{5}} \tag{7}$$

Therefore, when the fiber diameter is fixed, $1/A'$ scales with $A^{-1/5}$. The results in Fig. 5**(c)** show that φ_{fm} is proportional to $A^{-1/5}$, indicating that φ_{fm} of the flexible fiber can also be represented by the original A. This can be used to make an estimate of φ_{fm} for flexible fibers. Certainly, further data acquisition is required to substantiate this conclusion.

4.3. Static yield stress

The relationship between the obtained relative yield stress and the corresponding relative fiber volume fraction ($\varphi_f^{'}$) is shown in Fig. 6. First, it can be clearly seen that the yield stress of FFRCP exhibits a step-like characteristic. When $\varphi_f^{'}$ is less than about 0.3, the yield stress of the material is close to the suspending cement paste, which means that the influence of fiber on the rheological properties of cement paste is relatively low at this time. However, as soon as the relative volume fraction exceeds this critical point, the relative yield stress of FFRCP increases dramatically by orders of magnitude. Furthermore, the theoretical value obtained by Eq. (1) is much smaller than the experimental results, especially at high fiber content. Therefore, unlike the situation where the maximum packing fraction of flexible fibers is measured using shear rheology at low fiber content, there may be other factors besides fiber straightening and rearrangement that contribute to the static yield stress of FFRCP.

It should be emphasized that the fiber content of samples subjected to static yield stress test in this study ranged from 1 to 3 %, although the maximum $\varphi_f^{'}$ ($L=12$ mm, φ_f=3%) is 0.6196. This value is smaller than the critical random loose packing fraction (0.8, the yield stress increases by an order of magnitude when $\varphi_f^{'}$ is greater than this value) defined in previous studies [12,20], i.e., the cut-off point for the degree of fiber influence on the rheological properties of the cement paste. It was found that the cementitious material was difficult to flow during the actual slurry preparation process at this time. Further analysis using crowding factor (N, defined as the number of fibers present in a spherical volume with a diameter equal to the length of one fiber) [48] and effective-medium theory (EMT) [49] showed that the selected PP fiber content basically exceeded the flocculation thresholds (Φ_f) for the formation of flocculation (Fig. 7). It can be presumed that the formation of the fiber flocculation network may be responsible for the experimental values

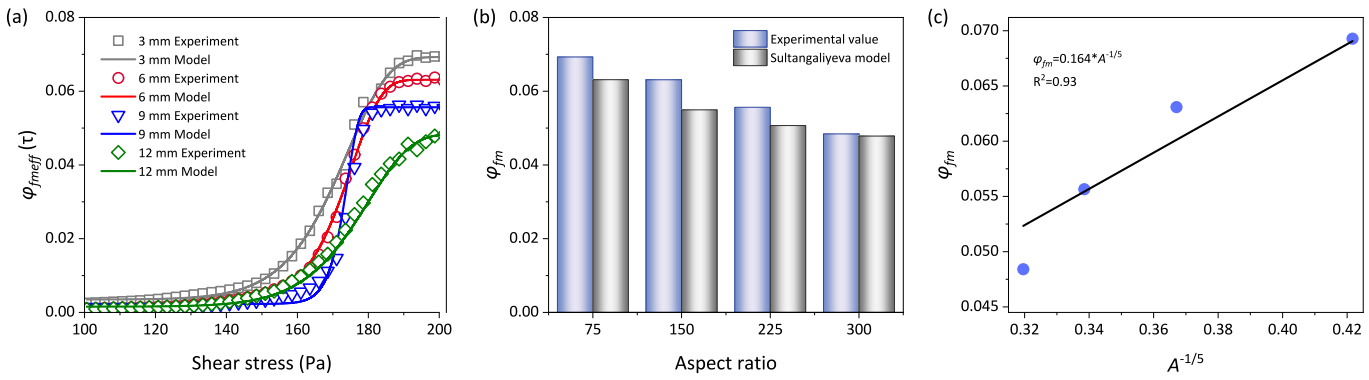

Fig. 5. (a) The effective maximum packing fraction $\varphi_{fmeff}(\tau)$ as a function of shear stress τ. (b) Comparison of the results in this study with the Sultangaliyeva model values. (c) Relationship between the maximum packing fraction φ_{fm} and $A^{-1/5}$.

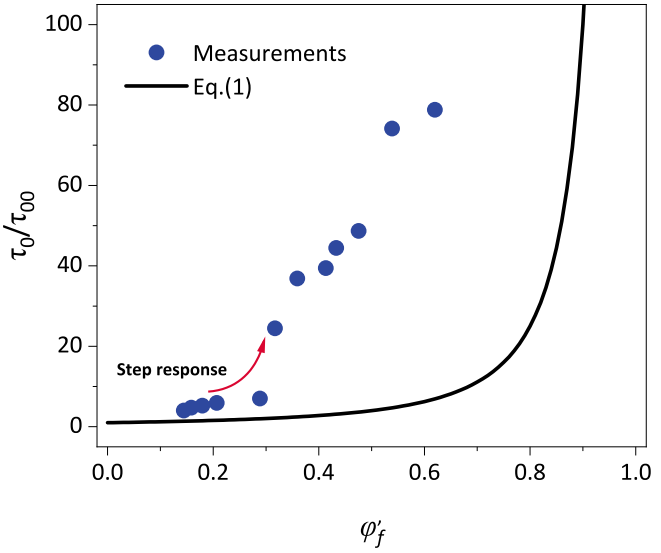

Fig. 6. Relative yield stress $\frac{\tau_0}{\tau_{00}}$ (both experimental and theoretical values) as a function of the relative volume fraction $\varphi_f^{'}$.

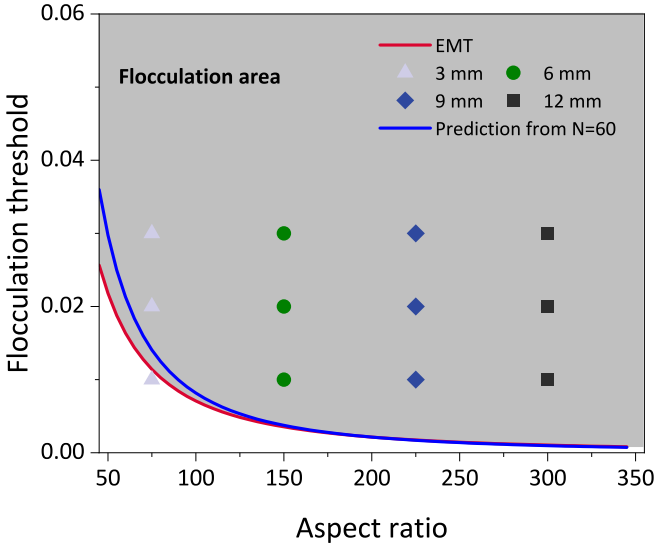

Fig. 7. Flocculation thresholds (Φ_f) calculated from the crowding factor N and EMT. The formulas for calculating the Φ_f based on the crowding factor and EMT are $\Phi_f = \frac{60}{\frac{2}{3}A^2}$ and $\Phi_f = \frac{36L_c(1-L_c)}{2+L_c(15-9L_c)}$ respectively, where $L_c = \frac{1-e^2}{2e^3}\left[ln\frac{1+e}{1-e} - 2e\right]$ and $e = \sqrt{1-(1/A)^2}$. More details can be found in [49].

being much larger than the theoretical answers of Eq. (1). The interlocking of fibers within the fiber flocculation restricts the free flow of fibers while allowing the fiber network to withstand certain external load [50]. The main sources of mechanical strength of fiber network are the mechanical surface linkage and the cohesive forces caused by the bending of the elastic fibers, i.e., the hooking force generated by the mechanical entanglement of fibers (Fig. 8**(a)**) and the frictional resistance induced by the normal forces at the contact points when the elastically bent fibers cannot be straightened due to contact with other fibers [50] (Fig. 8**(b)**). These cohesive forces are particularly pronounced at high fiber volumetric concentration. Therefore, the gap ($\Delta\frac{\tau_0}{\tau_{00}}$) between the above experimental results and the model values of Eq. (1) could be mainly attributed to the hooking and friction effects between the fibers in the fiber network.

According to the classical beam theory, the shear stress caused by friction is only related to A and φ_f, while the stress caused by mechanical surface linkage can be expressed by the number of contacts per fiber ($n = \sqrt{\frac{A^2\varphi_f}{8\pi}}$) [52]. Furthermore, the solid contact contribution can be given by a power law, i.e., $\propto\mu^c\varphi_f^{'2}$ (μ^c is the contact coefficient) [53]. In addition, a strong linear correlation is observed when plotting $\Delta\frac{\tau_0}{\tau_{00}}$ against $\varphi_f^{'}$, which $\propto\varphi_f A^{1/5}$, on a log–log scale (Fig. 9**(a)**). Therefore, $\Delta\frac{\tau_0}{\tau_{00}}$ can be regarded as a power function of $\varphi_f^{'}$ for simplicity. At the same time, the following model was firstly proposed by introducing a step function $\beta\left(\varphi_f^{'}\right)$ to capture the step characteristics of the yield stress of FFRCP:

$$\frac{\tau_0}{\tau_{00}} = \beta\left(1-\varphi_f^{'}\right)^{-2} + (1-\beta)\Delta\frac{\tau_0}{\tau_{00}} = \beta\left(1-\varphi_f^{'}\right)^{-2} + \rho(1-\beta)\varphi_f^{'h} \tag{8}$$

where ρ and h are constants related to fiber properties such as elastic modulus, the β can be expressed as:

$$\beta = 1 - \frac{1}{1+exp\left[-q\left(\varphi_f^{'} - \varphi_{f0}^{'}\right)\right]} \tag{9}$$

This step function makes β equal to 0 or 1 when $\varphi_f^{'}$ is greater or less than the transition point $\varphi_{f0}^{'}$ and q (here taken as 100) determines the sharpness of the equation [54].

Next the parameters of the equation are determined from the experimental data and the final relative yield stress model of FFRCP is given by:

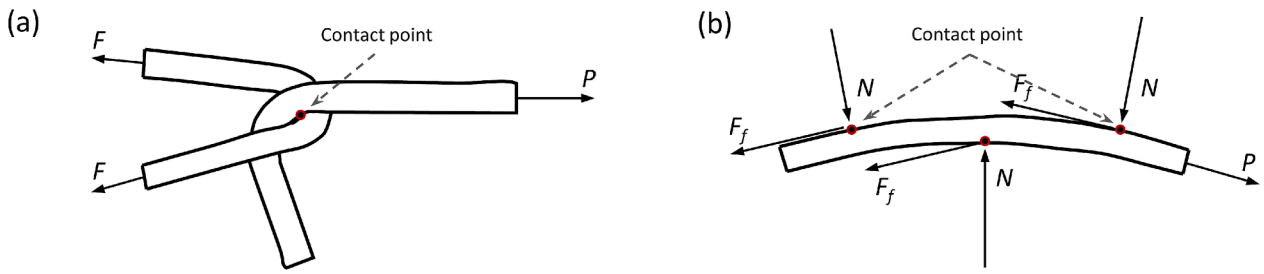

Fig. 8. Cohesive forces (P) caused by (a) hooking of whole fibers and (b) bending of elastic fibers (adapted from [51]). N is the normal force, F_f is the friction force.

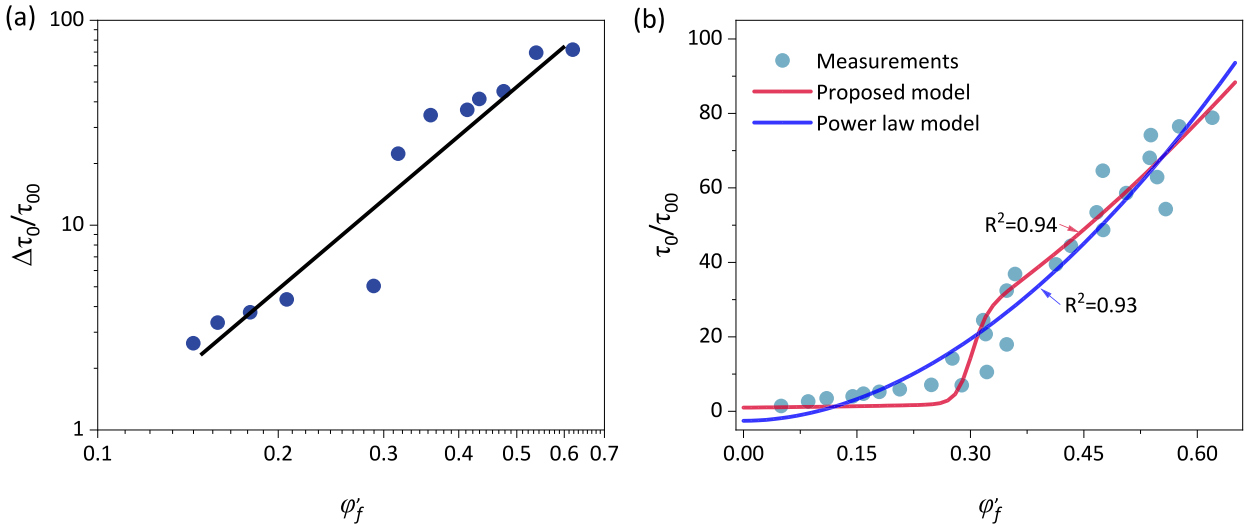

Fig. 9. (a) Log – log plot of relative yield stress difference $\Delta\frac{\tau_0}{\tau_{00}}$ versus the relative volume fraction φ_f'. (b) Correlation between predicted and experimental relative yield stress $\frac{\tau_0}{\tau_{00}}$.

$$\frac{\tau_0}{\tau_{00}} = \left\{1 - \frac{1}{1+exp\left[-100\left(\varphi_f' - 0.299\right)\right]}\right\}\left(1-\varphi_f'\right)^{-2} + 176.909\left\{1 - \left\{1 - \frac{1}{1+exp\left[-100\left(\varphi_f' - 0.299\right)\right]}\right\}\right\}\varphi_f'^{1.612} \quad (10)$$

From Eq. (10), it can be found that when the relative fiber content is less than φ_{f0}' (0.299), the equation can be simplified to Eq. (1), which is consistent with the experimental results in Fig. 6. At this time, the interaction of fibers in the flexible fiber flocculation network can be ignored, and the yield stress enhancement effect of fibers mainly comes from the straightening and rearrangement of fibers. This is also the principle of using shear rheology to measure the maximum packing fraction of flexible fibers, and it also explains the reason why the premise of this method is low fiber content. When the relative fiber volume fraction is greater than φ_{f0}' Eq. (1) is no longer applicable. At this point the total shear stress sustainable by the fiber network will be mainly given by the entanglement and frictional effects of the fibers.

To verify the accuracy and applicability of the proposed model, FFRCP with different fiber aspect ratios and contents were prepared and the static yield stress tests were carried out. The theoretical predictions were compared to the experimental values, and the results are shown in Fig. 9**(b)**. The correlation coefficient R^2 reaches 0.94 indicating that a good agreement has been achieved. A P-value 1.31E-17 (<0.01) indicates a significantly different distribution between experimental values and model values. It should be noted that the modeling slightly underestimates the experimental values when φ_{f0}' ranges from 0.1 to 0.299, indicating that the fiber interaction cannot be completely ignored at this time, which needs to be improved in the future. However, this does not contradict the underlying logic of the proposed measurement method for the maximum packing fraction of flexible fibers, as the fiber content selected for the experiments is sufficiently low. In addition, the fitting results of the simple power law model ($y = a_1 + b_1 \bullet x^{c_1}$, a_1, b_1 and c_1 are the fitting parameters respectively) are also shown in Fig. 9 **(b)**. Although this model also provides a good description of the relative yield stress and is easy to use, the fitting parameters are not linked to the fiber–fiber interactions and some important features such as step response are not represented. The proposed model is able to take into account the effect of fiber and capture the evolution characteristics of yield stress, so it is a more ideal model.

4.4. Structural build-up

Structural build-up of various FFRCPs was evaluated using static yield stress test and dynamic rheology (Fig. 10). As shown in Fig. 10**(a)**, FFRCP exhibits higher static yield stress compared to pure cement paste regardless of the resting time. In addition, the structural build-up rate increases with increasing fiber length or aspect ratio. For example, FFRCPs containing fibers with lengths of 3, 6, 9 and 12 mm have corresponding A_{thix}^{FFRCP} of 0.0613, 0.0647, 0.0756 and 0.1202 Pa/s respectively. This can be attributed to the spatial congestion within the fiber network [55]. As noted earlier, longer fibers correspond to a smaller φ_{fm}. Therefore, a longer length implies a higher relative fiber volume fraction for a given fiber content. Thus, an increase in the number of contact points between fibers leads to an increase in A_{thix}^{FFRCP}. Similar observations were also made by Rubio et al. for the fiber cement-based materials [56].

The evolution of G' and δ is shown in Fig. 10**(b) and (c)**. The

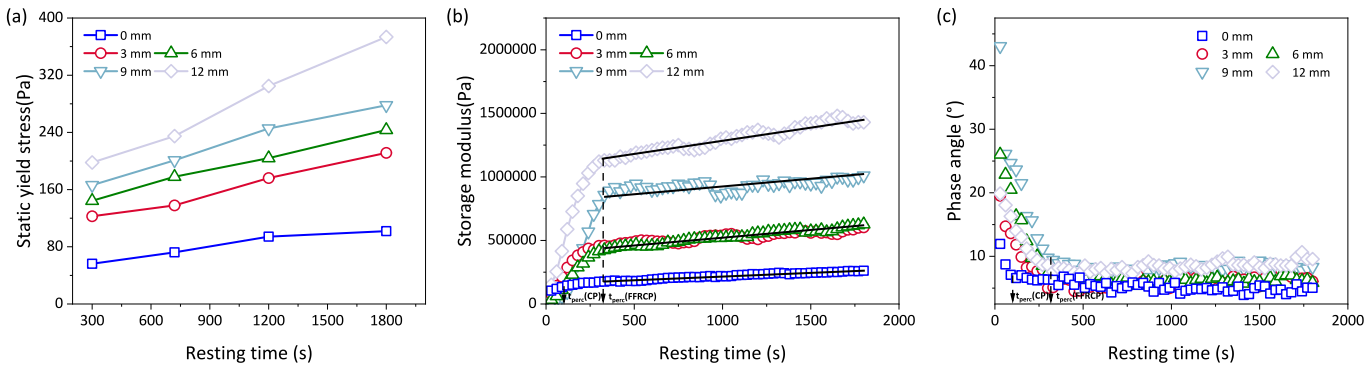

Fig. 10. Evolutions of (a) static yield stress, (b) storage modulus G′ and (c) phase angle δ with resting time for FFRCPs with fiber content of 1%.

structural build-up of FFRCP suspensions is characterized by an increase in G′ accompanied by a decrease in δ during an initial certain rest period, after which G′ increases linearly while the evolution of δ becomes insignificant. Since the pre-shear step is not performed, the system does not reach a good dispersion state reflected by G′ has a certain initial value. However, the mixing, transfer and rotor immersion steps inevitably destroy the sample. Therefore, the particle flocculation network is formed under the van der Waals attraction [57], which is reflected by an increase in G′ and a decrease in δ, i.e., the transition from a liquid-like state to a solid-like state. After a certain resting time, the percolation time (t_{perc}), the colloidal particles reach the favourable equilibrium position, and δ remains stable [58]. The volume of hydration products formed during the period may increase linearly as in Refs. [57,59], resulting in a linear increase in G′ with time [60], and the G′ evolution rate is also called the rigidification rate (G_{rigid}). In the following, the kinetics of build-up of FFRCPs is examined in more detail using G_{rigid} and t_{perc} according to Mostafa and Yahia [58].

As expected, incorporation of fibers results in greater G′ (i.e., higher rigidity) (Fig. 10**(b)**). This is in good agreement with the static yield stress results. Compared with the pure cement paste (57.664 Pa/s), the addition of fibers increases G_{rigid} values with the fiber lengths being 116.158, 115.263, 117.655 and 207.489 Pa/s respectively, but the G_{rigid} does not increase strictly with fiber length as in the case of A_{thix}^{FFRCP}. The G_{rigid} of FFRCP is almost the same when the fiber lengths are 3, 6 and 9 mm, while it increases significantly when the fiber length increases to 12 mm. This may be related to the higher number of contact points in the fiber network when the fiber length is 12 mm. It should be noted that a larger G_{rigid} does not mean faster formation of the colloidal network, i.e., a smaller t_{perc}. In fact, pure cement paste exhibited the shortest t_{perc} (105 s), while the determined percolation times for FFRCPs were around 320 s, regardless of the fiber length. A similar phenomenon was also found in cement-based suspensions with polycarboxylate high-range water-reducer (HRWR) [58]. t_{perc} is not affected by the degree of hydration and can be used solely to describe the physical structural changes [61]. One possible reason for this is that the incorporation of fibers increases the separation distance between particles due to the wall effect [62].

To gain further insight into the modeling of the structural build-up of FFRCP, the experimental relative yield stress (τ_0/τ_{00}), relative structural build-up rate ($A_{thix}^{FFRCP}/A_{thix}^{CP}$, A_{thix}^{CP} is the structural build-up rate of cement paste) and the prediction values of the Perrot model [31] were compared, as shown in Fig. 11. The Perrot model describes the structural build-up of rigid fiber-reinforced cement-based materials well. Firstly, it can be seen that the predicted results of the Perrot model are significantly lower than the actual values. The structural build-up has a strong correlation with the inclusion contacts and crowding effects [63]. Therefore, the underestimation of the Perrot model results can be attributed to the higher internal friction and fiber interlocking effect of the flexible fiber network, which can deform more than a rigid fiber

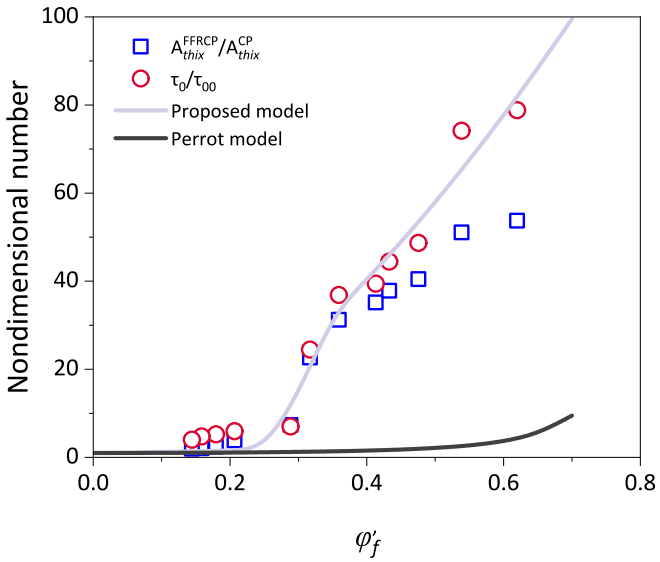

Fig. 11. Non-dimensional structural build-up and yield stress as a function of relative fiber volume fraction and the comparison with the predictions of the Perrot model [31].

network [64]. In addition, the discrepancy between the relative yield stress and the relative structural build-up rate continues to increase with the relative fiber volume fraction, reflected by the relative structural build-up rate presenting lower values. For rigid fiber reinforced cement-based materials, τ_0/τ_{00} and $A_{thix}^{FFRCP}/A_{thix}^{CP}$ start to deviate only when the relative volume fraction is larger than the random loose packing fraction (0.8) [31]. This implies that both types of fibers limit the structural build-up, but to varying degrees. Similar to particle flocs, flexible fibers are more prone to form complex contact networks trapping free water or cement particles due to the ease deformability compared to rigid fibers. This is the reason why flexible fibers limit the structural build-up of FFRCP from a low content (φ_{f0}'). Fig. 11 shows that the relative yield stress and structural build-up rate of FFRCP follow a similar trend as a function of the relative fiber volume fraction ranging from 0 to φ_{f0}'. Therefore, the structural build-up rate of FFRCP can be written as $A_{thix}^{FFRCP} = A_{thix}^{CP} \bullet \frac{\tau_0}{\tau_{00}}$ at this point. Due to the restriction effect of the fibers, the structural build-up rate of FFRCP deviates from the relative yield stress, and further investigation into modeling the structural build-up for relative volume fractions higher than φ_{f0}' is required in future work.

5. Conclusions

In this study, a method for measuring the maximum packing fraction

(φ_{fm}) of flexible fibers based on shear rheology was proposed. The micro-CT was utilized to preliminarily verify the conformation hypothesis of the fiber under shear. Then, a yield stress model for flexible fiber-reinforced cement paste (FFRCP) was established to interpret entanglement and friction effects in the fiber network. Finally, the static yield stress test and the small amplitude oscillatory shear (SAOS) test were performed to investigate the structural build-up of FFRCP. Based on the results of this study, the following conclusions can be drawn:

1. When the shear stress is less than 150 Pa, the effective maximum packing fraction ($\varphi_{fmeff}(\tau)$) is almost independent of the shear stress, regardless of the length or aspect ratio of the flexible fibers, due to the fibers' adaptability to deformation. Subsequently, $\varphi_{fmeff}(\tau)$ continues to increase until it reaches the φ_{fm}, corresponding to the optimal fiber conformation. The dynamic characteristics of the packing fraction of flexible fibers can be described by a stretched exponential function (Eq. (6)). The rheology-based method proposed can directly and accurately measure the φ_{fm} of flexible fibers, but the applicable premise of this method is low fiber content to avoid the influence of fiber–fiber interaction.
2. When the relative fiber volume fraction ($\varphi_f^{'}$) is less than 0.299, the enhancement effect of flexible fibers on yield stress of FFRCP primarily arises from the straightening and rearrangement of fibers. When $\varphi_f^{'}$ exceeds 0.299, the entanglement and frictional effects of the fibers become dominant factors. The proposed yield stress model (Eq. (10)) can take into account the fiber–fiber interactions and effectively quantify the yield stress characteristics of FFRCP.
3. The addition of fibers increases the structural build-up rate (A_{thix}^{FFRCP}) and rigidification rate (G_{rigid}), but G_{rigid} does not increase strictly with fiber length as A_{thix}^{FFRCP} does. Although FFRCP can form the elastic network faster compared to pure cement paste, the percolation time of FFRCP does not depend on fiber length. In addition, when $\varphi_f^{'}$ is less than 0.299, the relative yield stress and structural build-up rate of FFRCP follow a similar trend as a function of $\varphi_f^{'}$. When $\varphi_f^{'}$ is greater than 0.299, the relative yield stress increases faster than the relative structural build-up due to the restriction effect of the flexible fiber network.

The findings of this study can enhance the understanding of the effect of flexible fibers on the rheology of cement paste, thereby providing a theoretical foundation for the mix design of FFRCP. It is worth noting that a relatively high W/C was used in this study, which can easily lead to segregation and bleeding. The applicability of the proposed shear rheology-based method as well as the static yield stress model in FFRCP with low W/C needs to be further studied, and this is also a subject of future work.

CRediT authorship contribution statement

Zhenbang Guo: Formal analysis, Investigation, Methodology, Validation, Writing – original draft. **Jingping Qiu:** Resources, Validation. **Duanping Huang:** Investigation, Methodology, Writing – review & editing. **Kai Liu:** Methodology, Writing – review & editing. **Alex Kirichek:** Writing – review & editing, Validation, Formal analysis. **Chen Liu:** Investigation, Validation, Writing – review & editing. **Boyu Chen:** Writing – review & editing, Investigation, Validation. **Yingliang Zhao:** Writing – review & editing, Validation, Investigation. **Zhengyao Qu:** Supervision, Resources, Conceptualization, Writing – review & editing.

Declaration of competing interest

The authors declare that they have no known competing financial interests or personal relationships that could have appeared to influence the work reported in this paper.

Acknowledgments

Financial supports by Key Research and Development Project of Liaoning (2020JH1/10300005), National Key Research and Development Program (2019YFC1907202), and China Scholarship Council (No. 202206080032) are greatly appreciated. The authors also would like to thank Fan Yao from Shiyanjia Lab (www.shiyanjia.com) for technical support of rheological tests.

Data availability

Data will be made available on request.

References

[1] Zhao S, Liu R, Liu J, Yang L. Comparative study on the effect of steel and plastic synthetic fibers on the dynamic compression properties and microstructure of ultra-high-performance concrete (UHPC). Compos Struct 2023;324:117570.
[2] Sabzi J, Esfahani MR, Ozbakkaloglu T, Gholampour A, Masoodi AR. Rehabilitation of reinforced concrete beam: Sustainable restoration mortar with waste materials. Case Stud Constr Mater 2024;20:e02827.
[3] Rezaiee-Pajand M, Sobhani E, Masoodi AR. Free vibration analysis of functionally graded hybrid matrix/fiber nanocomposite conical shells using multiscale method. Aerosp Sci Technol 2020;105:105998.
[4] Yoo D-Y, Kim S, Park G-J, Park J-J, Kim S-W. Effects of fiber shape, aspect ratio, and volume fraction on flexural behavior of ultra-high-performance fiber-reinforced cement composites. Compos Struct 2017;174:375–88.
[5] Yang Y, Zhou Q, Deng Y, Lin J. Reinforcement effects of multi-scale hybrid fiber on flexural and fracture behaviors of ultra-low-weight foamed cement-based composites. Cem Concr Compos 2020;108:103509.
[6] Banthia N, Sappakittipakorn M. Toughness enhancement in steel fiber reinforced concrete through fiber hybridization. Cem Concr Res 2007;37:1366–72.
[7] Mohr BJ, Nanko H, Kurtis KE. Durability of kraft pulp fiber–cement composites to wet/dry cycling. Cem Concr Compos 2005;27:435–48.
[8] Arunachalam SK, Muthiah M, Rangaswamy KD, Kadarkarai A, Arunasankar CG. Improving the structural performance of reinforced geopolymer concrete incorporated with hazardous heavy metal waste ash. World J Eng 2021.
[9] Azenha M, Schlicke D, Benboudjema F, Jkedrzejewska A. SynerCrete'18: interdisciplinary approaches for cement-based materials and structural concrete: synergizing expertise and bridging scales of space and time 2018;vol. 1.
[10] Kumar Dwivedi V, Kumar D. Graphene as a stimulus for mechanical strength in glass-fiber reinforced polymers composite. World J Eng 2023;20:143–9.
[11] Margabandu S, Subramaniam SK. Influence of fiber stacking sequences and matrix materials on mechanical and vibration behavior of jute/carbon hybrid composites. World J Eng 2021;19:639–51.
[12] Martinie L, Rossi P, Roussel N. Rheology of fiber reinforced cementitious materials: classification and prediction. Cem Concr Res 2010;40:226–34.
[13] Martinie L, Rossi P, Roussel N. Rheology of Fiber-reinforced Cementitious Materials: Basic Concepts and Application to UHPFRC. Des Build with UHPFRC 2011:575–8.
[14] Mehdipour I, Libre NA, Shekarchi M, Khanjani M. Effect of workability characteristics on the hardened performance of FRSCCMs. Constr Build Mater 2013;40:611–21.
[15] Arunkumar K, Muthiah M. Invention of sustainable geopolymer concrete made with low calcium waste wood ash. World J Eng 2022;19:843–53.
[16] Yuan Q, Xie Z, Yao H, Huang T, Li Z, Zheng X. Effect of polyacrylamide on the workability and interlayer interface properties of 3D printed cementitious materials. J Mater Res Technol 2022;19:3394–405.
[17] He L, Chow WT, Li H. Effects of interlayer notch and shear stress on interlayer strength of 3D printed cement paste. Addit Manuf 2020;36:101390.
[18] Xiao J, Ji G, Zhang Y, Ma G, Mechtcherine V, Pan J, et al. Large-scale 3D printing concrete technology: Current status and future opportunities. Cem Concr Compos 2021;122:104115.
[19] Li LG, Chu SH, Zeng KL, Zhu J, Kwan AKH. Roles of water film thickness and fibre factor in workability of polypropylene fibre reinforced mortar. Cem Concr Compos 2018;93:196–204.
[20] Sultangaliyeva F, Carré H, La Borderie C, Zuo W, Keita E, Roussel N. Influence of flexible fibers on the yield stress of fresh cement pastes and mortars. Cem Concr Res 2020;138:106221.
[21] Li LG, Zhuo HX, Zhu J, Kwan AKH. Packing density of mortar containing polypropylene, carbon or basalt fibres under dry and wet conditions. Powder Technol 2019;342:433–40.
[22] Gwon S, Han SH, Vu TD, Kim C, Shin M. Rheological and Mechanical Properties of Kenaf and Jute Fiber-Reinforced Cement Composites. Int J Concr Struct Mater 2023;17:5.
[23] Zhang K, Pan L, Li J, Lin C, Cao Y, Xu N, et al. How does adsorption behavior of polycarboxylate superplasticizer effect rheology and flowability of cement paste with polypropylene fiber? Cem Concr Compos 2019;95:228–36.
[24] Lee S-J, Ryu S, Won J-P. Relationship between the rheology and flowability of self-compacting structural synthetic fibre-reinforced cementitious composites. Compos Struct 2021;267:113862.

[25] Fung WWS, Kwan AKH, Wong HHC. Wet packing of crushed rock fine aggregate. Mater Struct Constr 2009;42:631–43.
[26] Wong HHC, Kwan AKH. Packing density of cementitious materials: Part 1-measurement using a wet packing method. Mater Struct Constr 2008;41:689–701.
[27] Kwan AKH, Fung WWS. Packing density measurement and modelling of fine aggregate and mortar. Cem Concr Compos 2009;31:349–57.
[28] Si W, Cao M, Li L. Establishment of fiber factor for rheological and mechanical performance of polyvinyl alcohol (PVA) fiber reinforced mortar. Constr Build Mater 2020;265.
[29] Emdadi A, Mehdipour I, Libre NA, Shekarchi M. Optimized workability and mechanical properties of FRCM by using fiber factor approach: theoretical and experimental study. Mater Struct Constr 2015;48:1149–61.
[30] Jiao D, De Schryver R, Shi C, De Schutter G. Thixotropic structural build-up of cement-based materials: A state-of-the-art review. Cem Concr Compos 2021;122:104152.
[31] Perrot A, Lecompte T, Estellé P, Amziane S. Structural build-up of rigid fiber reinforced cement-based materials. Mater Struct 2013;46:1561–8.
[32] Chen M, Yang L, Zheng Y, Li L, Wang S, Huang Y, et al. Rheological behaviors and structure build-up of 3D printed polypropylene and polyvinyl alcohol fiber-reinforced calcium sulphoaluminate cement composites. J Mater Res Technol 2021;10:1402–14.
[33] Tregger NA, Pakula ME, Shah SP. Influence of clays on the rheology of cement pastes. Cem Concr Res 2010;40:384–91.
[34] Liu D-M. Particle packing and rheological property of highly-concentrated ceramic suspensions: φm determination and viscosity prediction. J Mater Sci 2000;35:5503–7.
[35] Abrishambaf A, Pimentel M, Nunes S. Influence of fibre orientation on the tensile behaviour of ultra-high performance fibre reinforced cementitious composites. Cem Concr Res 2017;97:28–40.
[36] Guo Z, Sun X, Zhang X, Qiu J, Jiang H, Zhao Y, et al. Effect of superplasticizer on rheology and thixotropy of superfine-tailings cemented paste backfill: Experiment and modelling. Constr Build Mater 2022;316:125693.
[37] Krieger IM, Dougherty TJ. A mechanism for non-Newtonian flow in suspensions of rigid spheres. Trans Soc Rheol 1959;3:137–52.
[38] Guo Z, Qiu J, Jiang H, Zhu Q, Kwek JW, Ke L, et al. Experimental and modeling study on the transient flow and time-dependent yield stress of superfine-tailings cemented paste backfill. Constr Build Mater 2023;367:130363.
[39] Liu J, Li C, Liu J, Cui G, Yang Z. Study on 3D spatial distribution of steel fibers in fiber reinforced cementitious composites through micro-CT technique. Constr Build Mater 2013;48:656–61.
[40] Ma S, Qian Y, Kawashima S. Experimental and modeling study on the non-linear structural build-up of fresh cement pastes incorporating viscosity modifying admixtures. Cem Concr Res 2018;108:1–9.
[41] Roussel N. Steady and transient flow behaviour of fresh cement pastes. Cem Concr Res 2005;35:1656–64.
[42] Alnahhal MF, Kim T, Hajimohammadi A. Distinctive rheological and temporal viscoelastic behaviour of alkali-activated fly ash/slag pastes: a comparative study with cement paste. Cem Concr Res 2021;144:106441.
[43] AbdelAleem BH, Ismail MK, Hassan AAA. Effect of Synthetic Fibers on Shear Capacity of Reinforced Rubberized Concrete Beams. ACI Mater J 2018;115.
[44] Mehdipour I, Libre NA. Linking fiber factor to material performance of fiber-reinforced self-consolidating cement-based materials. ACI Mater J 2017;114:77–91.
[45] Soua Z, Larue O, Vorobiev E, Lanoisellé J-L. Estimation of floc size in highly concentrated calcium carbonate suspension obtained by filtration with dispersant. Colloids Surfaces A Physicochem Eng Asp 2006;274:1–10.
[46] Han D, Ferron RD. Influence of high mixing intensity on rheology, hydration, and microstructure of fresh state cement paste. Cem Concr Res 2016;84:95–106.
[47] Kwan AKH, Fung WWS. Roles of water film thickness and SP dosage in rheology and cohesiveness of mortar. Cem Concr Compos 2012;34:121–30.
[48] Kerekes R, Schell C. Regimes by a crowding factor. J Pulp Pap Sci 1992;18:J32–8.
[49] Celzard A, Fierro V, Pizzi A. Flocculation of cellulose fibre suspensions: the contribution of percolation and effective-medium theories. Cellul 2008;15:803–14.
[50] Bennington CPJ, Kerekes RJ, Grace JR. The yield stress of fibre suspensions. Can J Chem Eng 1990;68:748–57.
[51] Kerekes RJ, Soszynski RM, Doo T. The flocculation of pulp fibres. Papermak. Raw Mater. Their Interact. with Prod. Process Their Eff. Pap Prop Eighth Fundam Res Symp held Oxford Sept 1985, 1985,:265–310.
[52] Wikstrorn T, Rasrnuson A. Yield stress of pulp suspensions. Nord Pulp & Pap Res J 1998;13:243–6.
[53] Boyer F, Guazzelli É, Pouliquen O. Unifying suspension and granular rheology. Phys Rev Lett 2011;107:188301.
[54] Shakeel A, Kirichek A, Talmon A, Chassagne C. Rheological analysis and rheological modelling of mud sediments: What is the best protocol for maintenance of ports and waterways? Estuar Coast Shelf Sci 2021;257:107407.
[55] Lecompte T, Perrot A. Non-linear modeling of yield stress increase due to SCC structural build-up at rest. Cem Concr Res 2017;92:92–7.
[56] Rubio M, Sonebi M, Amziane S. 3D printing of fibre cement-based materials: fresh and rheological performances. Acad J Civ Eng 2017;35:480–8.
[57] Roussel N, Ovarlez G, Garrault S, Brumaud C. The origins of thixotropy of fresh cement pastes. Cem Concr Res 2012;42:148–57.
[58] Mostafa AM, Yahia A. New approach to assess build-up of cement-based suspensions. Cem Concr Res 2016;85:174–82.
[59] Guo Z, Qiu J, Pel L, Zhao Y, Zhu Q, Kwek JW, et al. A contribution to understanding the rheological measurement, yielding mechanism and structural evolution of fresh cemented paste backfill. Cem Concr Compos 2023;143:105221.
[60] Huang T, Yuan Q, Zuo S, Li B, Wu Q, Xie Y. Evaluation of microstructural changes in fresh cement paste using AC impedance spectroscopy vs. oscillation rheology and 1H NMR relaxometry. Cem Concr Res 2021;149:106556.
[61] Mostafa AM, Yahia A. Physico-chemical kinetics of structural build-up of neat cement-based suspensions. Cem Concr Res 2017;97:11–27.
[62] Chu SH, Jiang Y, Kwan AKH. Effect of rigid fibres on aggregate packing. Constr Build Mater 2019;224:326–35.
[63] Lowke D. Thixotropy of SCC—A model describing the effect of particle packing and superplasticizer adsorption on thixotropic structural build-up of the mortar phase based on interparticle interactions. Cem Concr Res 2018;104:94–104.
[64] Assaad J, Khayat KH. Assessment of thixotropy of self-consolidating concrete and concrete-equivalent-mortar-effect of binder composition and content. ACI Mater J 2004;101:400–8.